PNAS
www.pnas.org

Supplementary Information for

Energetic regulation of coordinated leader-follower dynamics during collective invasion of breast cancer cells

Jian Zhang, Kayla F. Goliwas, Wenjun Wang, Paul V. Taufalele, Francois Bordeleau, Cynthia A. Reinhart-King

Corresponding author: Cynthia A. Reinhart-King
Email: cynthia.reinhart-king@vanderbilt.edu

This PDF file includes:

Supplementary Materials and Methods
Figures S1 to S4
Table S1
Captions for Movies S1 to S3
References for SI reference citations

Other supplementary materials for this manuscript include the following:

Movies S1 to S3
Dataset S1

www.pnas.org/cgi/doi/10.1073/pnas.1809964116

Supplementary Materials and Methods

Cell culture and plasmids

All cells were maintained in a humidified environment at 37 °C with 5% CO_2. MDA-MB-231 breast adenocarcinoma cells (HTB-26, ATCC, Rockville, MD) were maintained in DMEM with high glucose (25 mM; Life Technologies, Grand Island, NY) supplemented with 10% fetal bovine serum (FBS; Atlanta Biologicals, Flowery Branch, GA), 100 µg/mL streptomycin (Life Technologies), and 100 U/mL penicillin (Life Technologies). Breast cancer associated fibroblasts (CAFs) were kindly provided by Dr. Andra Frost (University of Alabama at Birmingham, Birmingham, AL) and were maintained in DMEM with low glucose (5.6 mM; Life Technologies) supplemented with 10% FBS, 100 µg/mL streptomycin, and 100 U/mL penicillin.

The CycleTrak plasmid (Fucci-Orange-G1/2A/H2B-eGFP) (1) was a gift from Dr. Paul M. Kulesa (Stowers Institute for Medical Research, Kansas City, MO). The photoactivatable mCherry plasmid (pPAmCherry1-N1, Addgene plasmid #31928) was a gift from Dr. Vladislav Verkhusha (Albert Einstein College of Medicine, Bronx, NY) (2), and expressed in the cell line through stable transduction using *Trans*IT-LT1 transfection reagent (Mirus Bio, Madison, WI) followed by selection with G418 (Corning, New York, NY). FUGW-PercevalHR (Addgene plasmid #49083) and GW1-pHRed (Addgene plasmid #31473) were kindly provided by Dr. Gary Yellen (Harvard Medical School, Boston, MA), and were coexpressed in the cell line through lentiviral transduction as described previously (3).

Spheroid and organoid preparation

MDA-MB-231 spheroids were generated as previously descried (4). Briefly, cells at approximately 80% confluency were harvested and resuspended in spheroid compaction medium containing 0.25% methylcellulose (H4100; Stem Cell Technologies, Cambridge, MA), 4.5% horse serum (Life Technologies), 18 ng/mL hEGF (Life Technologies), 0.45 µg/mL hydrocortisone (Sigma-Aldrich, St. Louis, MO), 9 µg/mL insulin (Sigma-Aldrich), 90 ng/mL cholera toxin (Sigma-Aldrich), 90 U/mL penicillin and 90 µg/mL streptomycin in DMEM/F12 (Life Technologies). The cell suspension was seeded into a 96-well round-bottom microplate with 5,000 cells in each well, which was then centrifuged at 300 × g for 5 min at room temperature. Spheroids formed in 2-3 days.

All mice were maintained following a protocol approved by the Vanderbilt University Institutional Animal Care and Use Committee. Tumor organoids were generated from MMTV-PyMT mice following published protocols (5). Briefly, mammary tumor tissues were harvested from 12-14-week-old mice and minced with a pair of scalpels. The minced tissues were then digested into small fragments at 37 °C for 30-50 min with collagenase solution containing 0.2% collagenase (Sigma-Aldrich), 0.2% trypsin (Life Technologies), 5 µg/mL insulin, 50 µg/mL gentamicin (Life Technologies) and 5% FBS in DMEM/F12. The digested tissues were harvested by centrifuging at 500 × g. The pellet was then treated with 2 U/µL DNase (Sigma-Aldrich) and differential centrifugation was applied to isolate organoids from single cells. Organoid culture medium contains 100 U/mL penicillin and 100 µg/mL streptomycin, 1% insulin-

transferrin-selenium (Life Technologies), and 2.5 nM bFGF (Life Technologies) in DMEM/F12.

Compacted spheroids or extracted organoids were added to 1.5 - 6.0 mg/mL collagen solution in complete culture medium, which was neutralized to pH = 7.0 with 1 N NaOH. Neutralized collagen solution (200 µL) with spheroids/organoids was pipetted into glass-bottom microplates (MatTek Corporation, Ashland, MA) and incubated at 37 °C for 30 min to induce polymerization. Embedded spheroids/organoids were allowed to invade for 1-3 days before imaging or treatment, with medium change every other day.

Immunofluorescence staining

Immunofluorescence images were acquired by fixing the cells with 3.7% formaldehyde (Sigma-Aldrich) in PBS and staining with a rabbit-anti-Ki67 antibody (Invitrogen, Carlsbad, CA) or a rabbit-anti-keratin 14 antibody (BioLegend, San Diego, CA). Cell nuclei were stained with DAPI (Invitrogen), and actin was labeled by Alexa Fluor 568 conjugated phalloidin (Invitrogen).

Microscopy

Static or time-lapse imaging were carried out with a Zeiss LSM800 confocal microscope, equipped with an environment control chamber. Time-lapse images were taken every 20 or 30 min for up to 20 h. A 10X dry lens N.A. = 0.3 was used to track cell nuclei within invading strands with 25-µm-interval Z-stacks and to image Ki-67 staining of cell proliferation. A 20X dry lens N.A. = 0.8 was used to monitor cellular ATP/ADP ratio along strands and extracellular 2-NBDG distribution with 6-µm-interval Z-stacks. A 40X water-immersion lens N.A. = 1.1 was used to image glucose uptake and keratin-14 staining along strands with 2-µm-interval Z-stacks.

Photo activation and FACS analysis

MDA-MB-231/pPAmCherry1-N1 spheroids were embedded in 4.5 mg/mL collagen. Following embedding, spheroids were imaged with a Zeiss LSM800 confocal microscope using a 20X dry lens N.A. = 0.8 and photoactivation was performed at a 3X zoom using the Zeiss Zen 2.3 software. The 405 nm laser was used to activate the cells at 20% laser power (20 iterations). After photoactivation, the spheroids were imaged every 12 h for up to 72 h. The percentage of strands with mCherry positive leaders was then quantified.

To isolate leader or follower cell subpopulations, spheroids were allowed to invade for 24 h before photoactivation of the leaders or the followers. After photoactivation, Accumax cell dissociation solution (Innovative Cell Technologies, San Diego, CA) was used to remove the cells from the collagen following the manufacturer's protocol. Single cell suspensions were analyzed via FACS for Texas Red and mCherry positive leader or follower cells were then sterilely collected. The isolated cell population were expanded, then either frozen down or used to generate secondary spheroids with 10% leaders and 90% followers.

Laser ablation of leader cells

MDA-MB-231 spheroids were embedded in 4.5 mg/mL spheroids and allowed to invade for 24 h. Spheroids were then imaged with a Zeiss LSM800 confocal microscope

using a 20X dry lens N.A. = 0.8 and leader cells were identified and ablated at 3X zoom using the Zen software. The 405 nm laser was used to ablate the leader cells at 70% laser power (75 iterations). After leader cell ablation, the strands were imaged every 12 h for up to 72 h. The length of the strand before and post ablation was measured over time using ImageJ.

Measurement of leader cell lifetime and cell migration within strands

To measure leader cell lifetime, MDA-MB-231 cells were lentiviral transduced to express the CycleTrak nuclear sensor (1) and tumor organoids were labeled with 0.5 μg/mL Hoechst 33342 to track the movement of cell nuclei. The invasion of each strand was tracked for a total of 14 h. A cell was identified as a leader if its nucleus was at the front of the strand. During leader/follower switching, the occurrence of a new leader was determined based on whether the far-end of its nucleus surpasses the far-end of the original leader's nucleus. As such, multiple leader cells can be identified for the same strand at different times. The duration between the first frame and last frame of a cell remaining as a leader was then defined as the lifetime of this leader cell. Leader cells that existed from the first frame or existed until the last frame of the 14-h tracking were considered as incomplete observations. The lifetime of all leader cells were then analyzed using Kaplan-Meier survival curves and incomplete observations were used as censored data in survival analysis. Only multi-cellular strands were analzyed for leader cell lifetime, whereas individually disseminated cells were not included.

Migration speed of individual cells within the strands was measured by tracking cell nuclei with the ImageJ (National Institutes of Health, Bethesda, MD) plugin, Tracking/Manual Tracking. Only cells tracked continuously for more than 5 h were analyzed. Velocity map of the strands was analyzed using the ImageJ plugin, PIV/iterative PIV (advanced). To make a kymograph of the velocity map, velocity vectors were projected to along the direction of the invading strand.

Measurement of glucose uptake

Glucose uptake was measured by incubating the spheroids/organoids with 0.146 mM of the fluorescent glucose analog 2-NBDG (Life Technologies) for 24 h, as previously described (3). The cells were then fixed with 4% paraformaldehyde (Sigma-Aldrich) in PBS. Due to light scattering in 3D imaging, the fluorescent intensities were usually attenuated toward the center of the spheroids/organoids. Ratio imaging was employed to normalize this effect, by labeling the cells with 10 μM CellTracker Orange CMRA dye (Life Technologies). MDA-MB-231 cells were labeled by incubating with the CellTracker Orange dye for 10 min before generating spheroids. Tumor organoids were labeled by incubating with the dye for 30 min and washing twice with PBS before 2-NBDG application. 2-NBDG was excited using a 488-nm laser whereas the CellTracker Orange dye was excited using a 561-nm laser. Pixel-over-pixel ratio of the 2-NBDG and CellTracker Orange images was then calculated as the normalized glucose uptake measurement. The average normalized glucose uptake was then measured at a blindly selected front region (leader position) and rear region (follower position) for each strand. To avoid complexity, only non-overlapping region of the strands were measured. To delineate cell boundaries, cell membrane was labeled with Alexa Fluor 633 conjugated WGA (Life Technologies) and imaged using a 640-nm laser.

To characterize the extracellular distribution of 2-NBDG, extracellular signals around unlabeled invading strands were imaged before 2-NBDG addition and monitored continuously for 24h after 2-NBDG addition. 0.1 mg/mL TRITC-dextran (Sigma-Aldrich) was added to the cell culture medium 24 h before imaging, which was used instead of the CellTracker Orange dye to normalize extracellular 2-NBDG concentration. The normalized extracellular 2-NBDG concentration was then evaluated along a 100-μm line parallel to the invading strand.

Measurement of intracellular ATP/ADP ratio

Cellular ATP/ADP ratio was measured in MDA-MB-231 cells using the PercevalHR probe and the pHRed probe, as previously described (3, 6). Briefly, two images were taken by exciting the PercevalHR probe with a 488- or 405-nm laser and emission light was collected over 410-546 nm range. Another two images were taken simultaneously by exciting the pHRed probe with a 561- or 488-nm laser and emission light was collected over 576-650 nm range. The ratio between the two PercevalHR images and two pHRed images were calculated pixel-by-pixel. Due to the pH sensitivities of the PercevalHR sensor (6), a calibration curve between PercevalHR ratio and pHRed ratio was measured to remove the bias caused by varying intracellular pH. 20 mM NH_4Cl was applied to the cell culture medium to induce a transient alkalization of the cytosol. Assuming that intracellular ATP/ADP ratio was maintained at a constant value during the short calibration period (2 - 3 min), a linear equation was fit from the calibration data, $r_{PercevalHR} = kr_{pHRed} + q$, where $r_{PercevalHR}$ and r_{pHRed} are the ratiometric values of the PercevalHR probe and the pHRed probe, and k and q are the slope and intercept of the fitted line, respectively. The linear equation was then used to correct the pH dependence, such that the corrected PercevalHR ratio became $r_{corr} = r_{PercevalHR} - kr_{pHRed}$. The corrected PercevalHR ratio was then normalized to the maximum of the entire time-lapse images unless otherwise stated and designated as the normalized ATP/ADP ratio, $r_{norm} = r_{corr} / \max\left(r_{corr}\right)$.

To determine the dynamics of ATP/ADP ratio in leader cells, the average ATP/ADP ratio within the front segment of each strand with a length of 25 μm along the direction of invasion was calculated. The cross-correlation between ATP/ADP ratio of the front segment and invasion was then calculated using the MATLAB (MathWorks, Natick, MA) function *crosscorr*.

To monitor leader-follower turnover events at the same time, the cells were labeled with 5 μM of the far-red nuclear dye DRAQ5 (Thermo Scientific, Waltham, MA), which was excited with a 640-nm laser and emission light was collected over 656-700 nm range.

Measurement of ATP concentration

Cellular ATP concentration was measured using the ATPLite luminescence assay kit (PerkinElmer, Waltham, MA) following the manufacturer's instruction. Briefly, MDA-MB-231 cells were seeded in 96-well plates with equal density and allowed to grow for 24 h. The cells were then treated with 200 μM AICAR (Sigma-Aldrich) to activate AMPK or switched to cell culture medium with DMEM containing 0 mM glucose (Life

Technologies). After 20 h of treatment, the cells were lysed with the lysis buffer and incubated with the luciferin/luciferase-based reaction buffer. The luminescent signal of each well was then detected using a microplate reader (BioTek Instruments, Winooski, VT). The luminescent intensity of each condition was normalized to the average intensity of the control group.

MDA-MB-231 cells with 0 μg or 1 μg exogenous mitochondria were seeded in 96-well plates with similar density 3 days after mitochondria transfer and allowed to grow for 24 h. The cells were then labeled with Hoechst and imaged to count cell numbers. Following ATPLite assay, the luminescent signals of each well were divided by the number of cells in each well.

Manipulation of cellular energy level

To increase cellular energy level, invading spheroids were preincubated with 200 μM AICAR for 4 h before starting imaging. To decrease cellular energy level, spheroids were preincubated in glucose-free medium before starting imaging. The effect of AICAR treatment and glucose starvation on cellular energy level was confirmed by monitoring ATP/ADP ratio every 2 min for 2 h post treatment for cells spreading on glass substrates.

Artificial mitochondria transfer and heterotypic spheroid generation

Mitochondria were isolated from donor CAFs using the Mitochondria Isolation Kit for Culture Cells (Thermo Scientific) following the manufacturer's instruction. Isolated CAF mitochondria were then transferred into MDA-MB-231 cells via centrifugation, as described previously (7). Briefly, isolated mitochondria were resuspended in 50 μL of PBS and kept on ice before use. Mitochondria concentration was determined using the DC protein assay (Bio-Rad Laboratories, Hercules, CA). The recipient MDA-MB-231 cells were pre-incubated with 20 mg/mL Pluronic F-68 (Life Technologies) for 2 h to increase membrane permeability. The recipient cells were then harvested and resuspended in PBS and kept on ice before transfer. 0 or 1 μg donor mitochondria were then transferred into 100,000 recipient cells by centrifugation at 1,500 × g, 4 °C for 5 min. The recipient cells were then labeled with the CellTracker Green CMFDA or CellTracker Orange CMRA dye, either seeded for ATPLite assay or mixed at 1:1 ratio to generate heterotypic co-culture spheroids.

Measurement of cell contractility and collagen strain

Cellular contractility within invading strands was evaluated using quantitative polarization microscopy as previously described (8). Briefly, a motorized linear polarizer (Thorlabs, Newton, NJ) was positioned in the illumination plane above the condenser of a Zeiss Axiovert microscope equipped with an Axiocam 506 color camera and a 20X polarization lens N.A. = 0.5. A circular polarizer was positioned in the imaging plane, and image sequences were acquired with 5-degree intervals of the rotating polarizer over a range of 0 to 180 degrees using the Zen software. The polarized image sequences were then processed with a custom MATALB code to obtain a pixel-by-pixel retardance map, The retardance signal, which is proportional to cell contractility (8), was then measured at both leader positions and follower positions after background subtraction.

To evaluate the strain field of collagen caused by cellular forces, 0.5 μm FluoSpheres fluorescent beads (Invitrogen) were added to the 4.5 mg/mL collagen matrix at 1:2,000 dilution. The spheroids were allowed to invade for 2 days before imaging using a Zeiss LSM800 confocal microscope. A 40X water-immersion lens N.A. = 1.1 was used to take 1-μm-interval Z-stack images of the beads and strands before stress relaxation. To release forces exerted on the collagen matrix, 0.5% Triton X-100 was added to the medium and a second Z-stack image was taken 2 h later. Bead displacements before and after stress relaxation were analyzed using the ImageJ plugin, Tracking/TrackMate, which were then interpolated to a regular grid and used to calculate the strain field using a custom MATLAB script.

Statistical analysis

Unless data were tested to be normal and variances were similar for groups being compared, nonparametric statistical tests were used. Two-sided tests were used wherever applicable. Statistical significance was identified if the tested *p*-value was smaller than 0.05(*), 0.01(**), 0.001(***), or 0.0001 (****). When multiple pairwise comparisons were performed, the Bonferroni correction was employed to adjust the significance level. All statistic tests were performed with Prism 6 (GraphPad Software, La Jolla, CA). Data are presented as mean ± s.e.m.

Computational modeling

A mathematical model of leader cell lifetime was built based on intracellular energy homeostasis. In the model, a cell at the front of a strand invades forward if its intracellular energy level, E, is above a threshold level, $E_{barrier}$. Intracellular energy level is maintained by the cell through a balance between energy generation and energy consumption, such that $dE/dt = G - C$, where G and C are the energy generation rate and energy consumption rate, respectively. Energy generation is controlled by multiple factors, including glucose concentration, AMPK activity, etc. For simplicity, we assumed that the factors we are interested in, i.e. glucose concentration and AMPK activity, have a linear effect on energy production whereas other factors were kept at a constant during our simulation and experiments, such that $G = G_0 + \gamma g + \theta_1 K$. Here, G_0 is a constant accounting for factors other than glucose concentration or AMPK activity, γ and θ_1 are proportional constants, g is glucose concentration, K is AMPK activity. Since AMPK is a sensor of cellular energy homeostasis (9), it is activated to increase energy production and reduce energy consumption when there is an energy crisis, we assumed that $K = K_0 + K_1 / E$, where K_0 and K_1 are constants. Energy consumption is also affected by multiple processes, such as the invasion rate, V, and AMPK activity. We also assumed a linear dependence for simplicity, such that $C = C_0 + \beta V - \theta_2 K$, where β and θ_2 are proportional constants, C_0 is a constant. For invasion to occur, the leader cell needs to overcome the energy barrier imposed from the surrounding extracellular matrix. We assumed that the energy barrier has a linear dependency on collagen density (3), such that $\bar{E}_{barrier} = E_0 + \alpha D$, where E_0 is a constant, α is the proportional constant, D is the density of the surrounding collagen matrix. To account for variabilities in energy barrier coming from factors other than collagen density, a white noise was added, such that

$E_{barrier} = N(\mu = \bar{E}_{barrier}, \sigma = \bar{E}_{barrier})$. Here $N(\mu, \sigma)$ represents a normal distribution with a mean of μ and a standard deviation of σ. To further simplify the model, we assumed that leader cells invade at a constant rate V_0 whenever $E > E_{barrier}$. Together, we obtained the following ordinary differential equation for controlling intracellular homeostasis, with $\theta = (\theta_1 + \theta_2)$,

$$\frac{dE}{dt} = (G_0 - C_0) + \gamma g - (E > E_{barrier})\beta V_0 + \theta(K_0 + \frac{K_1}{E}) \quad [1]$$

The above equation can be further simplified to have fewer parameters as follows

$$\frac{dE}{dt} = a + bg + \frac{c}{E}, a = G_0 - C_0 - (E > E_{barrier})\beta V_0 + \theta K_0, b = \gamma, c = \theta K_1 \quad [2]$$

Computer simulation of the above model was carried out using MATLAB. To start the simulation, at time *t = 0*, a tip cell was randomly assigned an initial energy level from a normal distribution, $N(\mu_E, \sigma_E)$, $\mu_E > E_{barrier}$. The evolvement of *E* was then controlled by *Eqn. 2*. The cell was considered to stop being a leader when $E \le E_{barrier}$, at time *t = T*. The duration, *T*, was then counted as the lifetime of this leader cell. Although this leader cell lifetime definition is slightly different from that used in experiments, they should correlate positively with each other. The simulation was run for 10,000 times for each condition, and the simulated lifetime data were plotted as survival curves. The parameters used for the simulations were listed in Table S1.

All data and associated resources used in this study are available upon request.

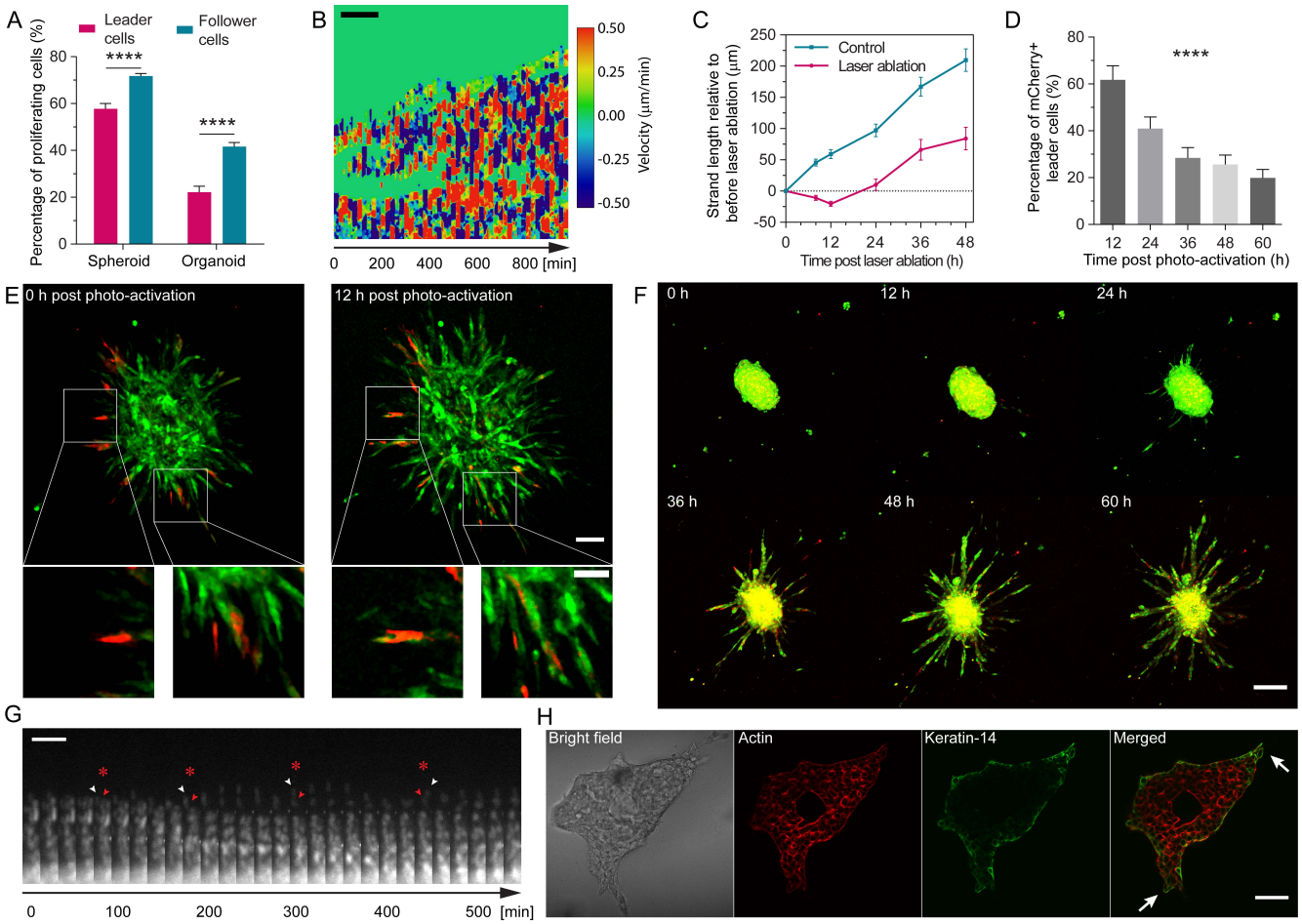

Figure S1. Characterization of leader and follower cells during breast cancer collective invasion *in vitro* and *ex vivo*. (A) The percentage of Ki67 positive proliferating cells is higher at the leader position compared to follower positions for MDA-MB-231 spheroid and MMTV-PyMT organoid invading in 4.5 mg/mL collagen (N > 250 cells for each condition; $p < 0.0001$ from unpaired t-tests for both comparisons). (B) Kymograph of migration velocity along invading direction of the strand as shown in Figure 1B. Scale bar, 50 μm. (C) Laser ablation of leader cells in MDA-MB-231 spheroids (at t = 0 h) results in temporary retractions of the strands, which recovered normal invasion 12 h later. (D) The percentage of photo-activated leader cells (activated at t = 0 h) decreases over time in MDA-MB-231 spheroids expressing a photo-activatable mCherry (N = 8-12 spheroids; $p < 0.0001$ from ANOVA test). (E) Photo-activated mCherry positive leader cells (red) are replaced by non-activated CellTracker-labeled follower cells (green) in 12 h. Scale bar, 100 μm (top), 50 μm (bottom). (F) Invasion of secondary MDA-MB-231 spheroids made up with 10% of FACS-isolated leader cells (red) and 90% of FACS-isolated isolated follower cells (green) after embedding into 4.5 mg/mL collagen (at t = 0 h). Note that FACS-isolated leader cells exist both at leader positions and follower positions. Scale bar, 200 μm. (G) A representative image of MMTV-PyMT organoid invading in 4.5 mg/mL collagen (hoechst-labeled) shows leader-follower turnover events (as indicated by asterisks; white arrow - new leader, red arrow - old leader). Scale bar, 50 μm. (H) Leader cells in MMTV-PyMT organoid and a few cells closely following the leaders are keratin-14 positive (as indicated by arrows). Scale bar, 50 μm.

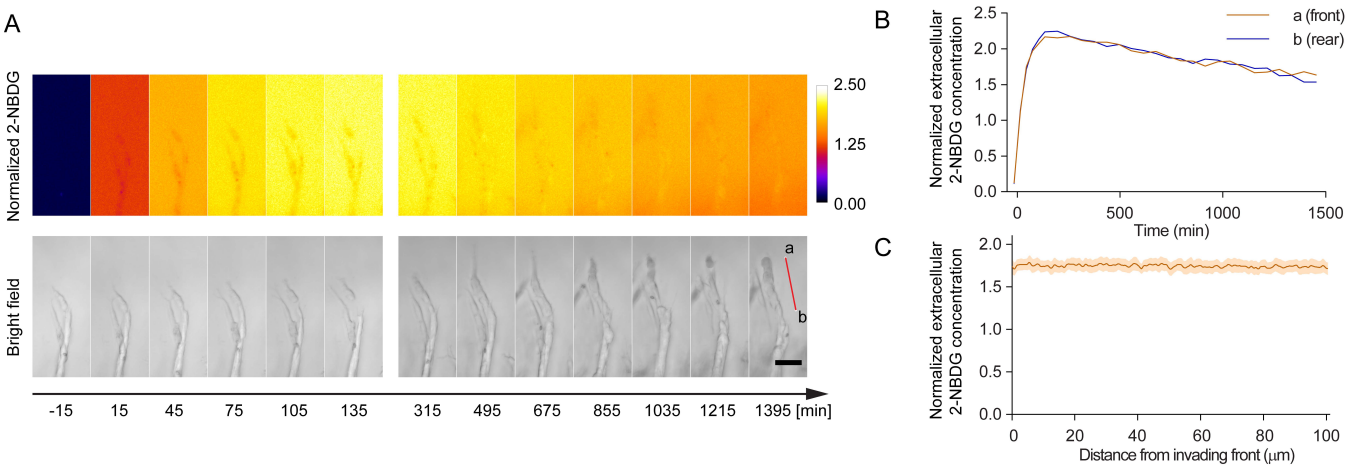

Figure S2. Characterization of extracellular glucose concentration. (A) Time-series image of normalized extracellular 2-NBDG (glucose analog) concentration and bright field image before and after the addition of 2-NBDG (at t = 0 min). (B) Normalized 2-NBDG concentration measured at a point close to the strand front (Point *a* in A) and another point close to the strand rear (Point *b* in A) suggests that extracellular 2-NBDG concentration changes over time due to diffusion but an apparent difference between front and rear never exists. (C) No apparent gradient in extracellular 2-NBDG concentration is observed along invading strands 24 h after 2-NBDG addition (averaged from N = 6 strands; shades represent s.e.). Scale bar, 50 μm.

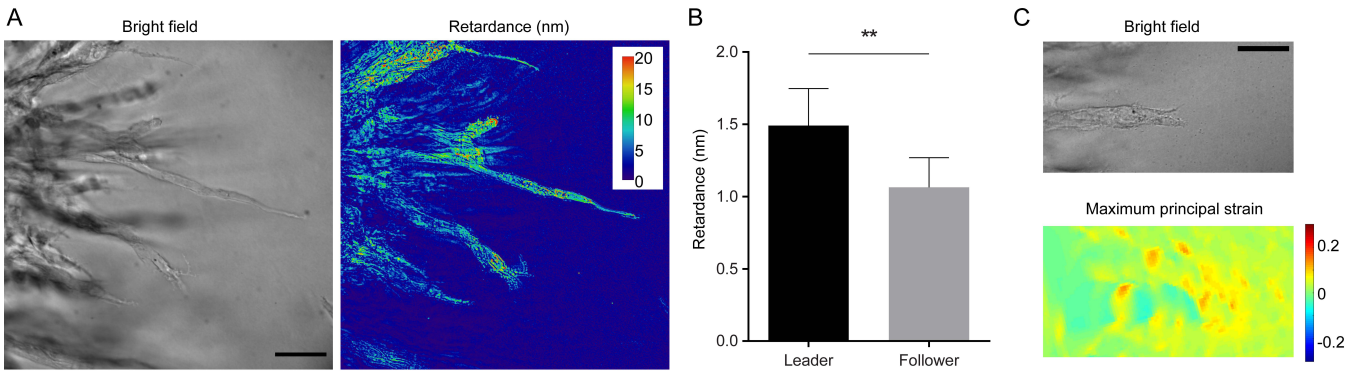

Figure S3. Cell contractility and matrix deformation. (A) A representative image of MDA-MB-231 spheroid invading in 4.5 mg/mL collagen and the corresponding heatmap of optical retardance. (B) Cell contractility as revealed by optical retardance is higher in leader cells than in follower cells (N = 23 strands; p = 0.0021 from Wilcoxon matched-pairs signed rank test). (C) A representative image of the collagen strain around an invading strand in 4.5 mg/mL collagen suggests that more strain energy is transmitted to the matrix near the leader than near the followers. Scale bar, 50 μm.

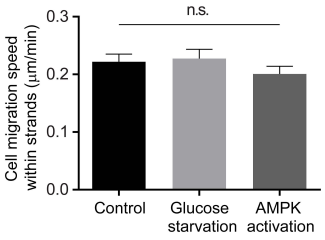

Figure S4. Migration speed of cells within invading strands. Migration speed of individual MDA-MB-231 cells within invading strand does not change with glucose starvation or AMPK activation (N = 72, 49 and 46, respectively; p = 0.3894 from Kruskal-Wallis test).

Table S1. Parameters used in model simulation

Variable	Value
a	-14 (when $E > E_{barrier}$)
b	0.2
c	500 (control), 750 (AMPK activation)
dt	1
D	1.5, 3.0, 4.5 (control), 6.0
E_0	20
g	0 (glucose starvation), 25 (control)
α	5
μ_E	100
σ_E	100

Movie S1. A representative MDA-MB-231 spheroid expressing the CycleTrak nuclear marker (green/yellow) is invading upward into 4.5 mg/mL collagen with collective strands, within which cells dynamically reorganize their relative positions.

Movie S2. A representative MMTV-PyMT organoid is invading into 4.5 mg/mL collagen with collective strands.

Movie S3. Bright-field images and heatmap images of normalized ATP/ADP ratio of a typical invading MDA-MB-231 strand in 4.5 mg/mL collagen indicate that cellular energy level correlates with leader cell invasion.

Dataset S1

Raw data of leader cell lifetime used to generate survival curves in Figure 1 and Figure 5.

References

1. Ridenour DA, McKinney MC, Bailey CM, Kulesa PM (2012) CycleTrak: A novel system for the semi-automated analysis of cell cycle dynamics. Dev Biol 365(1):189–195.
2. Subach F V., et al. (2009) Photoactivatable mCherry for high-resolution two-color fluorescence microscopy. Nat Methods 6(2):153–159.
3. Zanotelli MR, et al. (2018) Regulation of ATP utilization during metastatic cell migration by collagen architecture. Mol Biol Cell 29(1):1–9.
4. Carey SP, Starchenko A, McGregor AL, Reinhart-King CA (2013) Leading malignant cells initiate collective epithelial cell invasion in a three-dimensional heterotypic tumor spheroid model. Clin Exp Metastasis 30(5):615–630.
5. Nguyen-Ngoc K-V, et al. (2015) 3D culture assays of murine mammary branching morphogenesis and epithelial invasion. Tissue Morphogenesis, Methods in Molecular Biology (Methods and Protocols)., ed Nelson CM (Humana Press, New York, NY), pp 135–62.
6. Tantama M, Martínez-François JR, Mongeon R, Yellen G (2013) Imaging energy status in live cells with a fluorescent biosensor of the intracellular ATP-to-ADP ratio. Nat Commun 4(May):2550.
7. Kim MJ, Hwang JW, Yun C-K, Lee Y, Choi Y-S (2018) Delivery of exogenous mitochondria via centrifugation enhances cellular metabolic function. Sci Rep 8(1):3330.
8. Wang W, Miller JP, Pannullo SC, Reinhart-King CA, Bordeleau F (2018) Quantitative assessment of cell contractility using polarized light microscopy. J Biophotonics 11(11):e201800008.
9. Hardie DG, Ross FA, Hawley SA (2012) AMPK: a nutrient and energy sensor that maintains energy homeostasis. Nat Rev Mol Cell Biol 13(4):251–262.